# Effect of Cholesterol on the Properties of Phospholipid Membranes. 4. Interatomic Voids

**Marina G. Alinchenko,[†] Vladimir P. Voloshin,[†] Nikolai N. Medvedev,[†,∥] Mihaly Mezei,[‡,⊥] Lívia Pártay,[§] and Pál Jedlovszky*,[§]**

*Institute of Chemical Kinetics and Combustion, Siberian Branch of the RAS, Group of Supramolecular Structures, Institutskaya 3, R-630090 Novosibirsk, Russia, Department of Physiology and Biophysics, Mount Sinai School of Medicine, New York University, 1 Gustave L. Levy Place, New York, New York 10029, and Department of Colloid Chemistry, Eötvös Loránd University, Pázmány Péter stny. 1/a, H-1117 Budapest, Hungary*

*Received: April 8, 2005; In Final Form: June 20, 2005*

The properties of the interatomic voids present in fully hydrated dimyristoylphosphatidylcholine (DMPC)−cholesterol mixed membranes of different compositions are analyzed in detail using a generalized variant of the Voronoi−Delaunay method on the basis of computer simulation results. The systems investigated are chosen from both sides of the DMPC−cholesterol miscibility gap; the pure DMPC bilayer has also been included in the analysis as a reference system. The results obtained show that the empty space is organized in a more compact way, forming larger voids in the presence than in the absence of cholesterol. The voids located in the region of the rigid cholesterol rings become, on average, less spherical, oriented more parallel with the membrane normal axis with increasing cholesterol concentration, whereas an opposite effect of cholesterol is observed in the middle of the membrane among the chain terminal methyl groups. In general, the preferential orientation of the voids is found to strongly correlate with that of the molecules in the hydrocarbon phase of the membranes. The membranes are found to contain rather large voids, the volume of which can be an order of magnitude larger than the largest spherical cavities present in the systems. These voids are elongated or branching channels rather than big empty holes. The voids located among the DMPC and cholesterol molecules are lying preferably parallel with the membrane normal axis. The existence of such empty channels can be of great importance in the cross-membrane permeation of small, uncharged penetrants, in particular, of polar molecules.

## 1. Introduction

Hydrated phospholipid−cholesterol mixed bilayer membranes have been intensively studied in the past decade both by experimental methods[1−12] and by computer simulations.[13−28] The main scientific importance of studying these systems comes from the fact that both phospholipids and cholesterol are essential components of the membranes of the eukaryotic cells, and hence such mixed bilayer systems can be regarded as simplified models of biomembranes. All kinds of communications of the living cells with their environment involves either the membranes themselves or specific protein molecules embedded in the membrane. Therefore, a deep understanding of the interaction of living cells with their environment requires an atomistic level description of the properties of the membranes.

For this purpose, computer simulation methods can provide a unique tool, since in simulations the macroscopic properties of the system investigated are derived directly from its microscopic, atomistic level configurations. The computer simulation studies performed previously on phospholipid−cholesterol mixed bilayers involved systems covering a wide range of cholesterol concentrations, containing various saturated (e.g., dimyristoylphosphatidylcholine (DMPC),[14,15,18,23−25] dipalmitoylphosphatidylcholine (DPPC)[13,16,17,19,20−22,26,28]), and unsaturated (e.g., dioleylphosphatidylcholine (DOPC)[27]) phospholipid molecules, cholesterol[13−18,20−26] and cholesterol sulfate,[19] as well as domains formed by 18:0 sphingomyelin and cholesterol molecules that are embedded in the phospholipid membrane.[27] In these studies several properties of the membranes, such as the distribution of the density of the system and of various different atomic groups along the membrane normal,[16,17,19,20,23,26,27] the thickness of the bilayer,[23,27] the structure of the headgroup region,[18−21,25] the free area properties of the membrane,[25−27] lateral diffusion of the molecules,[13,16,22,26] the effect of the cholesterol molecules on the ordering of the lipid tails,[13,14,16−23,26,27] and the profile of the electrostatic potential[15−20,22] as well as of the solvation free energy of various small, uncharged molecules across the membrane[24] have been analyzed in detail.

One of the key functions of the biological membranes is to regulate the transport of molecules from one side to the other. While many of the penetrants, such as ions go through the membrane with the aid of specific membrane-bound channel-forming protein molecules, several small, uncharged molecules of physiological relevance (e.g., $O_2$, $CO_2$, CO, NO, $NH_3$, ...) can simply cross the membrane by passive diffusion. Due to

---

* To whom correspondence should be addressed. E-mail: pali@para.chem.elte.hu.
† Institute of Chemical Kinetics and Combustion, Siberian Branch of the RAS, Group of Supramolecular Structures, Institutskaya 3, R-630090 Novosibirsk, Russia.
‡ Department of Physiology and Biophysics, Mount Sinai School of Medicine, New York University, 1 Gustave L. Levy Place, New York, New York 10029.
§ Department of Colloid Chemistry, Eötvös Loránd University, Pázmány Péter stny. 1/a, H-1117 Budapest, Hungary.
∥ E-mail: nikmed@kinetics.nsc.ru.
⊥ E-mail: mezei@inka.mssm.edu.

Interatomic Voids in DMPC/Cholesterol Membranes

*J. Phys. Chem. B, Vol. 109, No. 34, 2005* **16491**

the key physiological role played by these molecules, understanding the principles governing their passive transport across the membrane is of great importance. However, the direct simulation of the cross-membrane diffusion of a penetrant is severely hampered by the large computational cost required by such a study. In fact, the diffusion profile of a few neutral penetrants across a lipid bilayer has, to our knowledge, only been estimated once from computer simulations, in the pioneering works of Marrink and Berendsen.[29,30] In our previous studies we have calculated the thermodynamic driving force of such transport, i.e., the variation of the solvation free energy of several penetrants along the membrane normal in a hydrated bilayer of pure DMPC[31] as well as of DMPC−cholesterol mixtures of various compositions.[24] However, in determining the permeability of the membrane for a given penetrant the thermodynamic background of its permeation (i.e., its solvation free energy profile) is complemented by the kinetic properties of the permeation (i.e., the diffusion profile) of the penetrant along the membrane normal axis.[29,30] The diffusion properties of the penetrant are largely determined by the distribution of the size and shape of the empty pockets, voids of the membrane. The analysis of the free volume properties of such complex, inhomogeneous, and anisotropic systems as hydrated lipid membranes have been, however, seriously limited by the difficulties in locating the voids in the system. The free volume properties of a hydrated phospholipid membrane has been analyzed in detail by Marrink et al.,[32] the fraction of empty volume across DPPC−cholesterol mixed membranes has been calculated by Tu et al.[16] and by Falck et al.,[26] whereas the density profiles of spherical cavities of different minimum radii have been determined across membranes of various compositions in our previous works.[24,31] Very recently Falck et al. have reported a detailed analysis of the voids in DPPC−cholesterol mixed membranes of low and moderate cholesterol concentrations.[28] In all of these studies cavities have been searched for along various grids. However, using a coarse grid in such analyses introduces a certain numerical inaccuracy in the results. To keep this numerical inaccuracy sufficiently low, a large number of grid points have to be used, which makes the entire analyses computationally rather costly. Furthermore, the computational cost of such calculations is proportional to the cube of the system size. The main advantage of searching for cavities along a grid is the simplicity of the procedure; however, one still has to face to the problem of identifying the voids in a lattice formed by a large number of occupied and unoccupied grid points. The possible algorithms that can be used for this problem are discussed in detail in the recent paper of Falck et al.[28]

Recently we have proposed to use for this purpose the Voronoi−Delaunay (VD) method,[33,34] which is able to map the voids very rapidly (i.e., its computational cost increases linearly with the system size) even in complex molecular systems.[35−38] To take into account the fact that the molecules in the membrane consist of atoms of different size, a generalized variant of the original VD method, based on the additively weighted Voronoi diagram,[37,39,40] has to be used. In this generalized variant of the Voronoi−Delaunay method, contrary to its classical form, the distance of a spatial point from an atom is regarded as the distance of the point from the *surface* rather than from the center of the atom. However, due to this definition the spatial regions assigned to given atoms (called the Voronoi S-regions), contrary to the classical Voronoi cells, are not polyhedra, which make their determination rather difficult in disordered molecular systems. Nevertheless, the Voronoi S-regions, confined by

hyperbolic faces, have been calculated several times in the past decade in order to use them for analyses concerning the molecular structure of the systems of interest.[41−46] The volume assigned to a given atom can certainly be defined in a physically more meaningful way by the Voronoi S-regions than by using either the classical Voronoi polyhedra or the radical (power) Voronoi cells.[47,48] However, in studying the interatomic voids the use of the Delaunay simplices seems to be more suitable. Every Delaunay simplex is determined by four mutually neighboring atoms and represents an elemental interatomic cavity.[33,34] Any complex void between the atoms of the system can be described as a cluster of these simplices.[35,49] The atoms forming the Delaunay simplices are defined by the Voronoi cells or, in the case of atoms of different size, by the Voronoi S-regions of the system. In this latter case these simplices are usually called Delaunay S-simplices.[35−37] Similarly to the classical Delaunay simplices, which have been studied with the aid of the classical Voronoi network several times,[35,50] the clustering of the Delaunay S-simplices can be studied in void analyses using the Voronoi S-network of the system, which is therefore a basic tool of such studies.[49,51]

Recently we have developed a novel and fast algorithm that enables the construction of the Voronoi S-network even in large, complex molecular systems.[36,37] In our previous studies, we have used this method to analyze the free volume properties of a fully hydrated DMPC membrane[36,37] as well as of hydrated membranes built up by various unsaturated phospholipid molecules[38] in detail. In this paper we present a detailed analysis of the free volume properties of DMPC−cholesterol mixed membranes of various compositions. The composition of one of the membranes investigated has been chosen from the cholesterol-rich, while that of another one from the cholesterol-poor side of the experimental DMPC−cholesterol miscibility gap located at 310 K between the cholesterol mole fraction values of 0.1 and 0.28.[3] For reference, the results obtained for the pure DMPC membrane are also presented. This study complements our recent investigations of the effect of cholesterol on various properties, such as the average membrane structure,[23] the ordering of the lipid tails,[23] the cross-membrane free energy profile of various small penetrants,[24] and the local lateral structure[25] of phospholipid membranes.

## 2. Computational Details

**2.1. Monte Carlo Simulations.** Details of the computer simulations performed have been described in our previous paper;[23] thus only a brief summary of them is given here. The simulations have been performed in the isothermal−isobaric ($N$, $p$, $T$) ensemble under physiological conditions, i.e., at 1 atm and 37 °C. Two mixed DMPC−cholesterol bilayers, chosen from both sides of the DMPC−cholesterol miscibility gap have been investigated. In addition, the pure DMPC membrane, regarded as a reference system, has been included in the analyses. Each side of the bilayer has contained 25 solute molecules, i.e., 25 DMPC in the first, 23 DMPC and 2 cholesterols in the second, and 15 DMPC and 10 cholesterols in the third system. These systems are referred to as the cholesterol-free, cholesterol-poor, and cholesterol-rich systems, respectively, throughout this paper. The bilayer has been hydrated by 2033 water molecules, represented by the rigid TIP3P potential model.[52] The DMPC and cholesterol molecules have been described by the CHARMM22 force field.[53] In the simulations these molecules have been treated in a semiflexible way; i.e., their bond lengths and bond angles have been kept fixed at their equilibrium values, whereas torsional flexibility

has been introduced. To maximize the lateral distance between two periodic images of the atoms, hexagonal prism-shaped basic simulation boxes have been used. Standard periodic boundary conditions have been applied.

The simulations have been performed by the program MMC.[54] In the simulations water displacements, solute moves, and volume change steps have been done in the following order. Every water displacement step has been followed by a solute move, and after every 625 pairs of such steps a volume change has been attempted. In a water displacement step a water molecule has been randomly translated in a random direction by no more than 0.3 Å and rotated around a randomly chosen space-fixed axis by an angle not larger than 20°. In selecting the water molecules to be moved, preferential sampling has been used; i.e., waters located closer to the bilayer have been selected with higher probabilities. In a solute move either, by 20% probability, an entire DMPC or cholesterol molecule has been translated randomly by no more than 0.05 Å and rotated randomly around a randomly chosen space-fixed axis, or, by 80% probability, a dihedral angle of the chosen molecule has been altered. The torsional angles to be changed have been selected in a sequential order, going from the end of the chains toward the middle of the molecules, but also subject to a probability filter allowing less frequent changes of the torsions located closer to the end of the chains.[55] Torsional changes as well as overall solute rotations have been made using the method of extension biased rotations;[55] i.e., the maximum angle of rotation has been determined according to the distance of the farthest rotated atom from the axis of rotation. In this way, units of smaller extension perpendicular to the axis of rotation have been, on average, rotated by larger angles than units of larger extensions.[55] The solute molecules have been chosen for move in a shuffled cyclic order.[56] In the volume change steps the volume of the basic simulation box has been changed by no more than 800 Å$^3$. To let the surface density of the bilayer be equilibrated independently of the total volume density of the system, in a volume change step either the cross-section of the system has isotropically been changed or the height of the prism-shaped basic box has been altered.[57] The two types of volume change steps have been performed in alternating order. The ratio of the accepted and tried moves has resulted in about 0.50, 0.25, and 0.35 for the water displacements, overall solute moves, and volume change steps, respectively, whereas 15−35% of the torsional rotations, depending on the torsional angle altered, have been successful. The systems have been equilibrated by performing $7 \times 10^7$ Monte Carlo steps. In the production phase of the simulations 1000 sample configurations, separated by $10^5$ Monte Carlo steps, each have been saved in each system for further analyses.

**2.2. Voronoi−Delaunay Analyses.** *2.2.1. The Voronoi S-Tessellation.* The classical Voronoi−Delaunay method,[33−35] working on a set of discrete spatial points (atomic centers) or spheres of equal radii, can find around each atom the region of space every point of which is closer to this central atom than to any other atom of the system. Therefore, a Voronoi cell can be assigned to the free volume available for the corresponding sphere, and these cells fill the space without gaps and overlaps.[33,34] The space-filling mosaic formed by the Voronoi cells is called the Voronoi tessellation[58,59] or Voronoi diagram.[39] An important property of the Voronoi tessellation is that it specifies quadruplets of mutually neighboring atoms. Each of these quadruplets, called Delaunay simplices, represents an elemental cavity. Any complex void present in the system is built up from such elemental cavities. Therefore, the classical

Voronoi−Delaunay method can be applied for the detailed analysis of the local environment of the particles as well as of the empty space between them in disordered phases of any kind of systems, the particles of which can be meaningfully modeled by simple spheres of equal radii. Thus, among others, the local structure of liquid metals,[60−64] molten[65,66] and supercooled salts,[67] systems of hard spheres,[68−73] Lennard-Jones particles,[61,74−76] or small molecules represented by a single Lennard-Jones sphere besides the distribution of the fractional charges (e.g., water,[77−82] hydrogen fluoride,[82] and $H_2S$,[77,81] etc.) have been analyzed in various respects (e.g., noncrystalline packings,[60,61,64,65,68−71,73,75,77−82] extended (i.e., intermediate range) structural correlations,[62,63,67,74] percolation and other properties of the interatomic voids, etc.[65,66,72,76,78]) by this method.

However, complex molecular systems (e.g., polymers, solutions of biomacromolecules, micelles, membranes, etc.) are built up by atoms of various sizes. This difference between the size of some of the constituting atoms can even be rather large. Further, chemically bound atom pairs approach each other much closer than the sum of their hard core or van der Waals radii. Hence, such systems can geometrically be represented as ensembles of partly overlapping spheres of different size. The partition of the space according to the closest sphere in such systems is far from being obvious. Clearly, the classical Voronoi−Delaunay approach cannot account for the differences of the atomic radii, and hence the partition of the space in this way can lose its original physical meaning of dividing the system into regions naturally assigned to the corresponding atoms. To retain the physical meaning of the original Voronoi tessellation, the method can be generalized in such a way that the distance of any point from an atom is measured from the surface rather than from the center of the atom. Then each cell, called the Voronoi S-region, is the locus of the spatial points that are closer to the surface of its central atom than to that of any other atom of the system. It can easily be proved that the Voronoi S-tessellation, i.e., the assembly of the Voronoi S-regions, also covers the space without gaps and overlaps.[35,39] Further, in the limiting case of atoms of equal radii the Voronoi S-tessellation coincides with the original Voronoi tessellation.

The faces, edges, and vertices of the Voronoi S-regions are the loci of points that are equally far from the surface of two, three, and four atoms, respectively, and are closer to the surface of these atoms than to that of any other atom of the system. Thus, the vertices are the centers of the empty interstitial spheres that can be inscribed between the atoms of the system. The quadruplets of atoms between which these empty spheres are inscribed are forming the Delaunay S-simplices.[35−37] Further, each edge of the Voronoi S-region connecting two of its vertices represents a "fairway" passing through the narrow bottleneck between the three nearest atoms. The set of vertices and edges of all the Voronoi S-regions of the system is forming a network that is called the Voronoi S-network. This network can be used to map the empty interatomic voids of the system.[37,49,51]

It should be noted that the Voronoi S-network of a system remains unchanged when the radius of all atoms of the system is decreased (or increased) by the same constant value (see Figure 2 of ref 37). This feature of the Voronoi S-network allows a rather straightforward treatment of the atomic overlapping.[37] Thus, the original system can be replaced by a reduced one by decreasing the radius of all the atoms by the same constant value that is large enough to eliminate all the atomic overlapping present in the system. Then the Voronoi S-network can be constructed on this reduced system of nonoverlapping spheres.

The algorithm used for constructing the Voronoi S-network[36,37] as well as the particular features of the Voronoi S-tessellation that should be taken into account in the construction procedure[35,37] are discussed in detail elsewhere.

*2.2.2. Determination of the Interatomic Voids.* The empty space between the atoms of a system is a complex, singly connected region confined between the atomic surfaces. Any interatomic void of the system is a part of this empty space. A physically meaningful definition of the interatomic voids is that regions of the empty space that are accessible for a spherical probe of the radius $R_{probe}$ are regarded as voids. Obviously, when using this definition, the voids that are present in a given system depend on the $R_{probe}$ value used, which should therefore be always indicated. The interatomic voids present in the system can be determined through the Voronoi S-network. Each site (vertex) of the Voronoi S-network is the center of an elemental spherical interstitial cavity, whereas each of its bonds (edges) represents the fairway passing through the bottleneck formed by a mutually neighboring atomic triplet. Thus, each site of the S-network can be characterized by the $R_i$ radius of the corresponding elemental interstitial cavity, whereas to each S-network bond the $R_b$ radius of its bottleneck (i.e., the distance of the surface of any of the corresponding three atoms from the closest point of the bond) can be assigned. Since the $R_b$ of a bond can never be larger than the $R_i$ of any of the two sites connected by this bond, a spherical probe of $R_{probe}$ can move along an S-network bond from one of its terminal sites to the other one if the relation $R_b \geq R_{probe}$ holds. Therefore, the probe can move along any clusters formed by Voronoi S-network bonds, the bottleneck radii of all of which exceeds the value of $R_{probe}$. Thus, such S-network clusters represent the "skeletons" of the interatomic voids, whereas the voids themselves are formed by the empty part of the Delaunay S-simplices corresponding to the S-network sites of these clusters. Details of the calculation of the empty part of the Delaunay S-simplices are discussed in our previous papers.[36,37]

It should be noted that the idea of using the parameter $R_{probe}$ for revealing voids accessible for a probe of a given size is related to the mathematical method called α-*shape*.[83] Indeed, both approaches use the full set of the Delaunay simplices of a system and perform a filtration of the Delaunay complex, i.e., an ordering of the simplices.[84,85] In our case it is done by the value of $R_{probe}$: for $R_{probe} = 0$ the entire empty intermolecular space is selected, whereas for rather large $R_{probe}$ values only the largest voids of the system are considered. Similarly, in the method of α-shape the parameter α governs the fictitious radii of atoms: $r_\alpha = \sqrt{r_0^2 + \alpha^2}$, where $r_0$ is the real radius of the atom. By increasing the radius of the atoms, they successively cover the empty space in the system from tight voids to the broad ones. Thus, from the mathematical point of view the two methods solve the same task, but their implementation and physical interpretation are different. The other difference of the two approaches is that here we use the additively weighed Voronoi diagram to define the Delaunay simplices instead of the radical one.

*2.2.3. Representation of the Voids by Spherocylinders.* To facilitate the analysis of the main characteristics (e.g., size, length, width, and orientation) of the interatomic voids found in lipid membranes, we have proposed to represent them by bodies of a relatively simple shape, namely, spherocylinders (i.e., cylinders covered by hemispheres of the same radii at the two basic circular faces).[36] This approach is justified by the fact that the voids detected by probes of reasonably large radius in the membrane are usually rather compact objects of elongated

shape. The algorithm of rapidly finding the spherocylinder that can best represent a given void has been described in detail in our previous papers,[36,37] and therefore it is only briefly summarized here. Thus, a fictitious mass proportional to the empty volume of the corresponding Delaunay S-simplex is assigned to each site of the Voronoi S-network cluster representing the void. Then the tensor of inertia of the cluster is calculated using the values of these fictitious masses. The axis of the spherocylinder is set as the axis along which the principal value of this tensor of inertia is minimal. The length of the cylindrical part of the spherocylinder $l$ is determined by projecting all the sites of the cluster to this axis and calculating the mean square deviation of these projections from the fictitious center-of-mass of the cluster (lying always along this axis). Finally, the radius $R$ of the spherocylinder (i.e., that of both the cylindrical part and the two hemispheres) is calculated by setting the volume of the spherocylinder equal to the volume of the void $V_{void}$, i.e., from the equation

$$V_{void} = R^2 \pi \left( l + \frac{4}{3} R \right) \tag{1}$$

where $V_{void}$ is the sum of the empty parts of the Delaunay S-simplices constituting the void. Obviously, the total length of the spherocylinder $L$ can simply be given as $L = 2R + l$. The sphericity of the void can be characterized by the parameter α, defined as

$$\alpha = \frac{2R}{2R + l} \tag{2}$$

for the corresponding spherocylinder. In the degenerate case when the spherocylinder is a perfect sphere (i.e., $l = 0$) α is equal to unity, and its value is smaller for more elongated spherocylinders. Finally, the orientation of a void relative to the membrane is characterized here by the cosine of the angle $\gamma$ formed by the axis of the corresponding spherocylinder and the bilayer normal.

## 3. Results and Discussion

**3.1. Total and Partial Profiles of the Free Volume.** The distribution of the voids across the membrane can be characterized by the total and partial profiles of the free volume. The total free volume profile is simply the fraction of the empty space along the bilayer normal axis $z$, whereas the partial profile corresponding to the value of $R_{probe}$ is the fraction of the volume of voids that are accessible for a spherical probe of this radius. Thus, the total profile of the free volume is equivalent with the partial profile corresponding to $R_{probe} = 0$. These profiles can be readily calculated from the empty volume of the Delaunay S-simplices, the interstitial sphere radius of which is larger than $R_{probe}$. The total profiles of the free volume obtained in the three systems investigated are shown in the top panel of Figure 1, whereas in the two lower panels of Figure 1 the partial profiles corresponding to the $R_{probe}$ values of 1.3 and 1.6 Å, respectively, are compared. All of the profiles shown are symmetrized over the two sides of the bilayer. Not surprisingly, the free volume profiles obtained correlate well with the mass density profile of the systems (see the top panel of Figure 2). Thus, in each case the fraction of the free volume is the lowest at about 20 Å away from the center of the bilayer. Considering the density profiles of various atomic groups (bottom panel of Figure 2), this part of the membrane can be assigned to the region of the zwitterionic headgroup of the DMPC molecules. The fraction of the empty space is considerably higher in the middle of the membrane among the hydrocarbon tails than in the headgroup
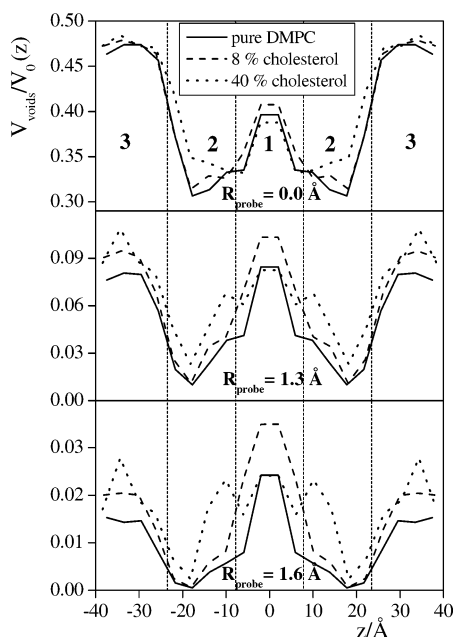
**Figure 1.** Total profile of the free volume (top) and partial free volume profiles corresponding to the probe radius values of 1.3 (middle) and 1.6 Å (bottom) across the three membranes investigated. Results obtained in the cholesterol-free, cholesterol-poor, and cholesterol-rich systems are shown as full lines, dashed lines, and dotted lines, respectively. All of the profiles shown are symmetrized over the two sides of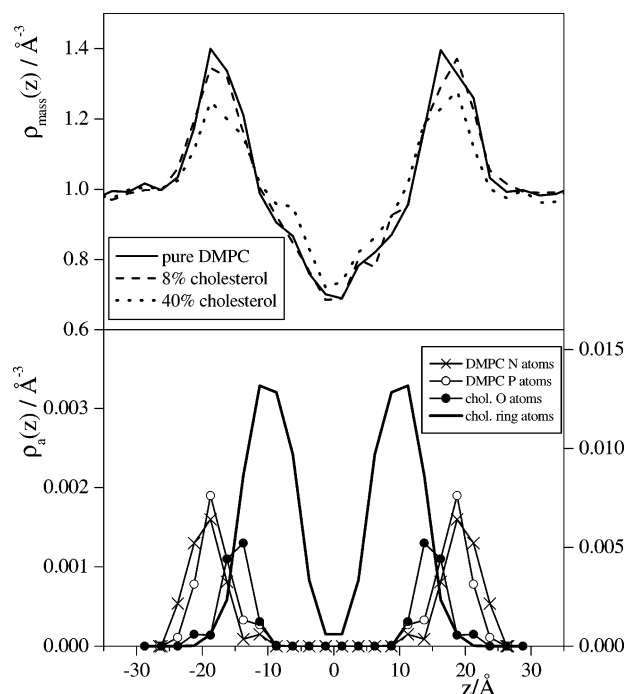 the bilayers. The dashed vertical lines illustrate the division of the systems into three separate regions on the example of the pure DMPC membrane.



**Figure 2.** Top: mass density profile of the three membranes simulated. Results obtained in the cholesterol-free, cholesterol-poor, and cholesterol-rich systems are shown as full lines, dashed lines, and dotted lines, respectively. Bottom: number density profile of the DMPC N (crosses) and P atoms (open circles), cholesterol O atoms (full circles), and cholesterol ring C atoms (solid line) across the cholesterol-rich system. All the profiles shown are symmetrized over the two sides of the bilayers.

region, and clearly the highest in the aqueous phase. According to the general behavior of these profiles we have divided the

membranes into three separate regions in a similar way as in our previous studies.[36,37] Thus, region 1, covering the middle 20% of the simulation box, is the apolar region of the hydrocarbon tails; region 2 is the rather inhomogeneous region of the glycerol backbones and headgroups (this region hosts also most of the cholesterol ring atoms), whereas region 3, defined as the farthest 20% of the simulation box from the bilayer center at both sides of the membrane, covers roughly the aqueous phase of the system. The division of the pure DMPC membrane to the above three regions is illustrated in Figure 1.

In analyzing the effect of cholesterol on the cross-membrane distribution of the entire empty space (top panel of Figure 1), it is seen that a small amount of cholesterol (i.e., at a concentration below the immiscibility region with DMPC) affects almost exclusively the $z$ range located between about $\pm 8$ and 15 Å ($z = 0$ Å being the middle of the membrane), where the density of the cholesterol ring atoms is high (see Figure 2). Here the fraction of the empty space is clearly increased by even a small amount of cholesterol molecules. However, in the presence of 40% cholesterol the fraction of the empty space is increased in a considerably broader $z$ range, between about $\pm 8$ and 25 Å, covering also the region of the phosphatidylcholine headgroups of the DMPC molecules (Figure 2), where the lack of the large headgroup of the cholesterol molecules leads to the creation of some empty space. These observations are also consistent with the mass density profiles of the systems (see Figure 2).

The effect of cholesterol on the fraction of the empty space in the middle part of the membrane is not trivial: as is seen from Figure 1, a small amount of cholesterol increases it, whereas in the cholesterol-rich system it becomes even somewhat lower than in the pure DMPC membrane. This behavior, however, correlates well with our previous observation on the dependence of the membrane thickness on the cholesterol concentration, namely, that in the presence of a small amount of cholesterol the membrane becomes thicker than in pure DMPC, whereas further increase of the cholesterol concentration above the immiscibility region makes the membrane even thinner than in the cholesterol-free system.[23] We have interpreted this behavior as the result of two opposite effects.[23] First, to fill, at least partly, the gap occurring due to the lack of the large polar headgroup of the cholesterol molecules in the region of the headgroups, the hydrogen-bonded DMPC neighbors of cholesterols prefer to stay farther from the bilayer center than the DMPC molecules located far enough from cholesterols. This effect is local and supposed to be noticeably strong only in systems of low cholesterol concentrations, i.e., when a sufficient amount of the DMPC molecules are still far enough from cholesterols. The fact that a few of the DMPC molecules prefer to stay noticeably farther from the bilayer center than the majority of them (see Figure 7 of ref 23) explains not only the increase of the average width of the bilayer but also the increase of the fraction of the empty space in the middle of the membrane. On the other hand, due to the lack of the second tail of the cholesterol molecule attached to its ring system, the flexible hydrocarbon chains of the DMPC molecules can extend more toward lateral directions in the middle of the membrane in the presence than in the absence of cholesterols.[23] Hence, the two membrane layers can approach each other closer, leading to the decrease of the free volume in the middle of the bilayer, and also to an overall thinning of the membrane. This effect is supposed to be stronger at higher fractions of cholesterol and hence to become dominant at high enough cholesterol concentrations, in a full accordance with our observations.
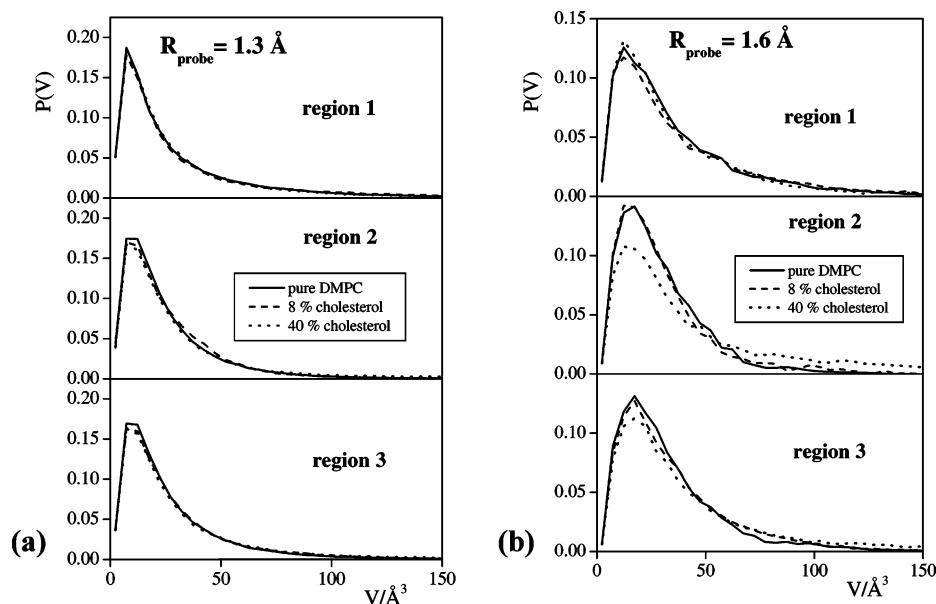
**Figure 3.** Distribution of the volume of the voids accessible for a probe of the radius of (a) 1.3 and (b) 1.6 Å in the three separate regions of the membranes simulated: solid lines, cholesterol-free system; dashed lines, cholesterol-poor system; dotted lines, cholesterol-rich system.

The distribution of the relatively large voids along the bilayer normal axis $z$ can be analyzed through the partial profiles of the free volume of the systems. The comparison of the profiles obtained with the $R_{probe}$ values of 1.3 and 1.6 Å with the total profiles (see Figure 1) show several important differences. Although all of the profiles obtained go through a minimum in the region of the headgroups and show maxima in the middle of the bilayer as well as in the aqueous phase, the relative height of the two maxima changes gradually with increasing probe radius. Thus, in the pure DMPC membrane the fraction of voids accessible for a given probe is roughly equal in the middle of the membrane and in the aqueous phase for the probe radius value of 1.3 Å and is clearly the highest in the bilayer center for $R_{probe} = 1.6$ Å. The systems containing cholesterol show a similar behavior with increasing $R_{probe}$ values. This finding indicates that the empty space is distributed considerably more uniformly in the aqueous than in the hydrocarbon phase of the membrane: although there is clearly more empty space in the aqueous phase, the density of the large voids is the highest in the apolar part of the membrane. Similar behavior has also been observed for various membranes built up by different saturated and unsaturated phospholipid molecules.[37,38]

It is also seen that, contrary to the fraction of the entire empty space, the fraction of the voids accessible for large enough probes is increased by the presence of cholesterol in all parts of the membrane. This finding indicates that cholesterol makes the distribution of the empty space more heterogeneous (i.e., forming larger voids) in the entire membrane.

**3.2. Properties of Large Voids.** The volume distribution of the voids present in the three separate regions of the systems simulated is shown in Figure 3 for the $R_{probe}$ values of 1.3 and 1.6 Å. As is seen, all the distributions look rather similar to each other. They are all peaked around 10 Å$^3$, whereas at large volumes they do not drop rapidly to zero, instead they exhibit a tail of exponential decay extending to rather large values. To better visualize the details of these tails, we have plotted the large volume part of the distributions obtained in the cholesterol-free and cholesterol-rich systems also on a logarithmic scale in Figure 4.

The comparison of the results obtained in the different parts of the membranes shows, consistently with our previous findings, that in the pure DMPC membrane the largest voids are clearly located in region 1, i.e., in the hydrocarbon phase of the membrane. In this region the effect of cholesterol on the size of the large voids is found to be marginal. This finding is in accordance with our former result that the chain terminal groups of the cholesterol and DMPC molecules are distributed in the same way along the membrane normal,[23] and hence cholesterol does not change considerably the structure of this membrane region. The situation is rather similar in the aqueous phase (region 3). Although in this region the fraction of the largest voids is somewhat larger in the cholesterol-rich than in the cholesterol-free system, this difference is probably due to the arbitrariness of the definition of the regions used and simply reflects the fact that in some cases region 3 contains also parts of the lipid headgroups. Contrary to regions 1 and 3, in the region of the headgroups (region 2) cholesterol has a clear effect on the size distribution of the largest voids: in the presence of a considerable amount of cholesterol the entire distribution is clearly extended to larger volumes, indicating the appearance of voids of the size that are absent in the absence of cholesterol. Furthermore, this effect becomes clearly more pronounced for larger $R_{probe}$ values. Thus, voids of the size of 180−400 Å$^3$ accessible for a probe of the radius of 1.3 Å, and of the size between 150 and 300 Å$^3$ accessible for a probe of $R_{probe} = 1.6$ Å are only present in this membrane region in the presence of a large amount of cholesterol. This fact is obviously related to the lack of the large polar group of the cholesterol molecule.

To understand the nature of these large voids, one should consider the fact that the systems do not contain a noticeable amount of spherical cavities larger than the radius of about 2 Å. This is illustrated by showing the distribution of the radii of the interstitial spheres of the Delaunay S-simplices $R_i$ in the three systems studied (see Figure 5). The fact that all the distributions drop to zero around 2 Å indicates that there is no void accessible for probes of the radius larger than this value in any part of the systems. The fact that the volume of even the largest spherical cavities present in the systems is not larger than about 35 Å$^3$ indicates that the large voids of the size of 50−400 Å$^3$ present in the systems are not big empty holes but rather narrow, elongated, or branched channels. This is illustrated in Figure 6, showing two of these large voids as picked
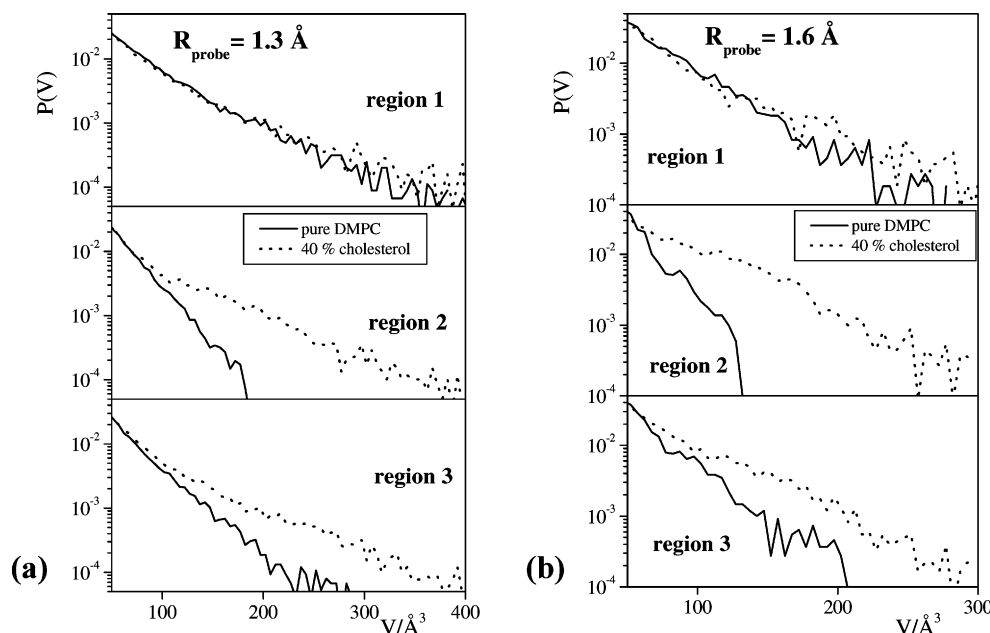
**Figure 4.** Distribution of the volume of the largest voids accessible for a probe of the radius of (a) 1.3 and (b) 1.6 Å in the three separate regions of the membranes simulated, shown on a logarithmic scale: solid lines, cholesterol-free system; dotted lines, cholesterol-rich system.
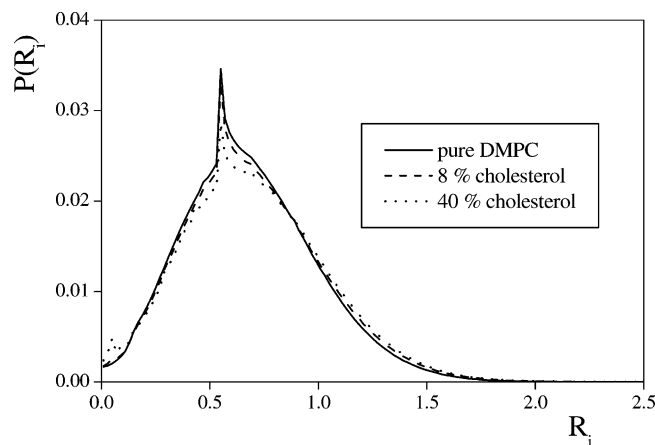


**Figure 5.** Distribution of the radii of the interstitial spheres of the Delaunay S-simplices $R_i$ in the three systems investigated.

up from two instantaneous configurations of the cholesterol-rich system. The fact that the volume of the large voids is strongly correlated with their length is demonstrated in Figure 7, showing the average volume of the voids $\langle V \rangle$ as well as the average length of the spherocylinders representing the voids $\langle L \rangle$ as a function of the probe radius $R_{probe}$ in the three regions of the cholesterol-free and cholesterol-rich system studied. The shape of the $\langle V \rangle (R_{probe})$ and $\langle L \rangle (R_{probe})$ curves are remarkably similar to each other in each case, although the volume of a void is calculated from the volume of the empty part of the constituting Delaunay S-simplices, i.e., in an exact way, whereas the values of $L$ are obtained from the somewhat arbitrary representation of the voids by spherocylinders.

**3.3. Percolation of the Voids.** In characterizing the properties of the empty space in the membrane, it is rather important to determine the critical probe radius $R_C$ below which the voids present in the system are percolating. However, due to the anisotropy of the membrane different $R_C$ values correspond to the percolation threshold in lateral and normal directions. Furthermore, the $R_C$ values can be different in the different regions of the membranes. In the present analysis, similarly to our previous studies[37,38] the value of the critical radius is defined separately for the lateral and normal percolation ($R_C^{XY}$ and $R_C^Z$,
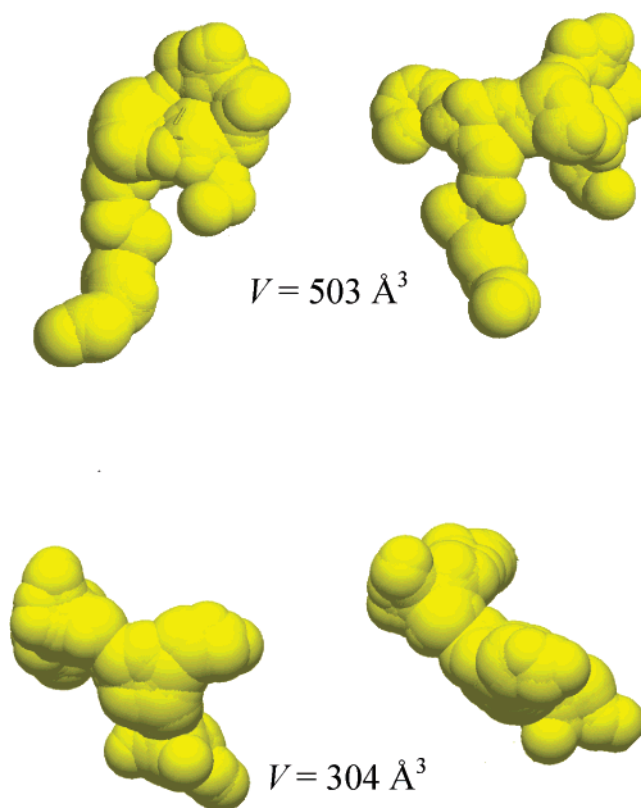


**Figure 6.** Large voids of the volumes of 503 (top) and 304 Å³ (bottom), both accessible for spherical probes of the radius of 1.3 Å, as picked up from instantaneous configurations of the cholesterol-rich system. Both voids are shown from two different views.

respectively) as the radius of the largest probe that can pass along a void from one side of the simulation box to the other one in the *xy* plane and along the *z* axis, respectively. The $R_C^{XY}$ and $R_C^Z$ values can also be defined for the separate membrane regions, with the only difference that now they represent the radius of the largest probe that have a lateral path across the system within the given region and a path between the boundaries of the region, respectively.
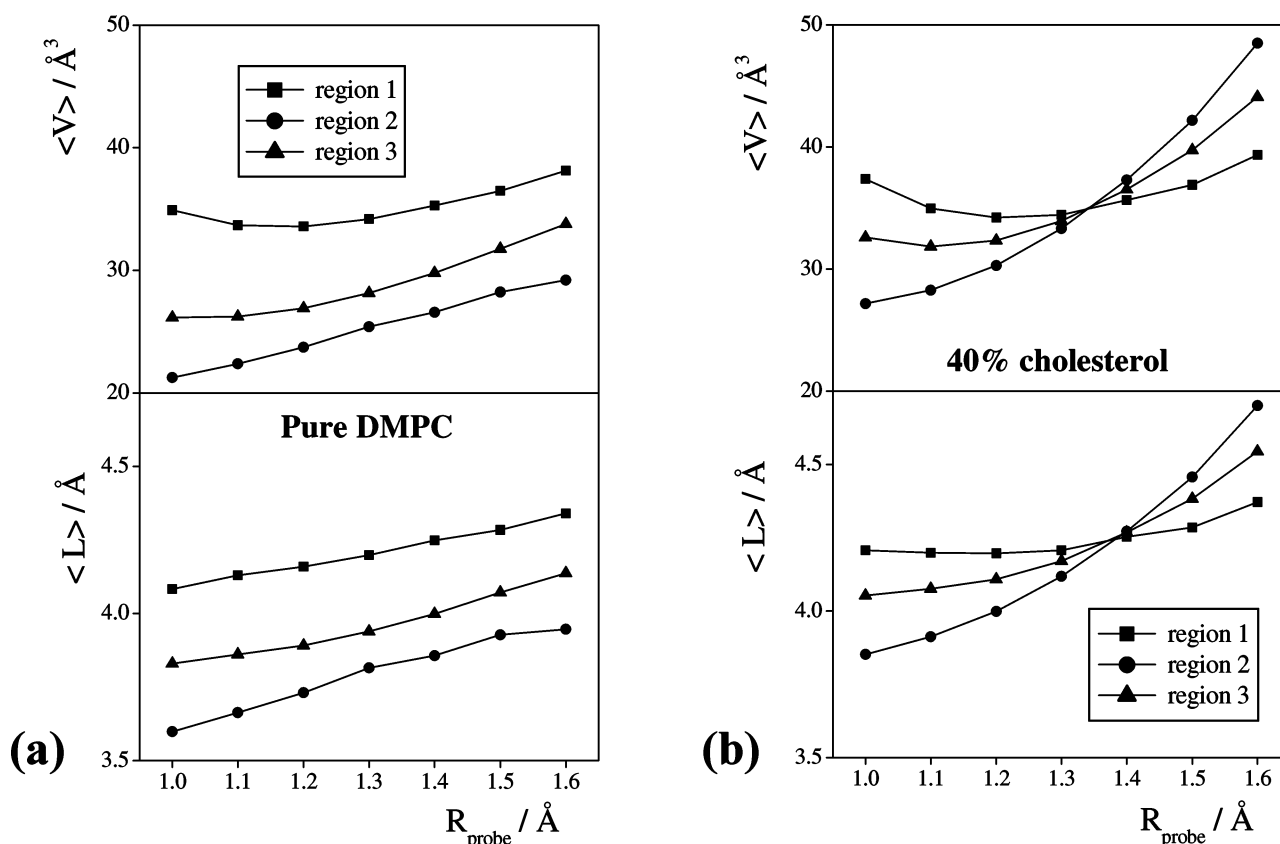
**Figure 7.** Average volume of the voids $\langle V \rangle$ and average length of the spherocylinders that are representing the voids $\langle L \rangle$ as a function of the probe radius (a) in the cholesterol-free system and (b) in the cholesterol-rich system.

**TABLE 1: Critical Normal Percolation Radius Values $R_C{}^Z$ as Obtained in the Three Systems Simulated as Well as In Their Separate Regions (All Values Are in Ångström Units)**

| mol % cholesterol | region 1 | region 2 | region 3 | entire system |
|---|---|---|---|---|
| 0 | $0.902 \pm 0.071$ | $0.692 \pm 0.050$ | $0.848 \pm 0.048$ | $0.648 \pm 0.027$ |
| 8 | $0.937 \pm 0.080$ | $0.700 \pm 0.061$ | $0.864 \pm 0.064$ | $0.660 \pm 0.036$ |
| 40 | $0.880 \pm 0.063$ | $0.782 \pm 0.064$ | $0.872 \pm 0.058$ | $0.712 \pm 0.027$ |

**TABLE 2: Critical Lateral Percolation Radius Values $R_C{}^{XY}$ as Obtained in the Three Systems Simulated as Well as In Their Separate Regions (All Values Are in Ångström Units)**

| mol % cholesterol | region 1 | region 2 | region 3 | entire system |
|---|---|---|---|---|
| 0 | $0.736 \pm 0.048$ | $0.573 \pm 0.028$ | $0.730 \pm 0.029$ | $0.782 \pm 0.029$ |
| 8 | $0.763 \pm 0.047$ | $0.583 \pm 0.031$ | $0.750 \pm 0.036$ | $0.808 \pm 0.036$ |
| 40 | $0.733 \pm 0.048$ | $0.631 \pm 0.032$ | $0.757 \pm 0.035$ | $0.810 \pm 0.030$ |

The $R_C{}^Z$ and $R_C{}^{XY}$ normal and lateral critical percolation radius values obtained in the separate regions as well as in the entire systems investigated are collected in Tables 1 and 2, respectively. As is seen, the $R_C{}^Z$ value of the entire system becomes somewhat larger for systems of higher cholesterol content. This is mostly due to the increase of the volume of the empty space and, particularly that of the relatively large voids in the dense region of the headgroups with increasing cholesterol concentration. This conclusion is based on the fact that the $R_C{}^Z$ values determined in region 2 show a similar dependence on the cholesterol concentration as the values characterizing the entire system. On the other hand, the $R_C{}^Z$ values obtained in region 1 do not depend noticeably on the cholesterol content of the membrane. Similarly, the $R_C{}^{XY}$ values are noticeably larger in systems of higher cholesterol content in region 2, whereas they do not show any clear dependence on the cholesterol concentration in region 1. It is also seen that in all of the three separate

membrane regions the values of $R_C{}^Z$ are considerably larger than $R_C{}^{XY}$; however, the opposite relation is observed between them when the entire systems are taken into account. Furthermore, the $R_C{}^Z$ values characterizing percolation in the entire system are always lower than the $R_C{}^Z$ values corresponding to any of the three regions of the same system, whereas $R_C{}^{XY}$ is always higher in the entire simulation box than in the separate regions of the system. These results indicate that (i) the size of the percolating channels along the $z$ axis is determined by their narrowest cross-section and (ii) the channels along which relatively large probes can move along lateral directions are also extended considerably along the membrane normal axis $z$. Thus, when limiting our analysis to a given slice of the system along the $z$ axis (i.e., to a given region), only some parts of these channels might be detected. Although these findings certainly suggest that the broad empty channels are likely to be oriented along the membrane normal axis rather than in lateral directions, such a definite conclusion cannot be drawn solely from the critical percolation radius values. However, this view can be supported by the $L_z(L)$ spot diagrams, shown for the three separate regions of the cholesterol-free and cholesterol-rich systems in Figure 8. In these diagrams each void is represented by a point, which corresponds to the total length of the spherocylinder representing the void $L$ and its extension along the membrane normal axis $L_z$. The position of a void along the $z$ axis has been taken as the $z$ coordinate of its fictitious center-of-mass, calculated using the empty volumes of the constituting Delaunay S-simplices as described in a previous subsection. The shown spot diagrams correspond to voids that are accessible for probes of the radius of 1.6 Å. As is seen, in the middle of the membrane (i.e., in region 1) the longest voids tend to align parallel with the membrane normal axis $z$ (as the points corresponding to large $L$ values are grouping close to

**pure DMPC membrane**　　**40 % cholesterol membrane**
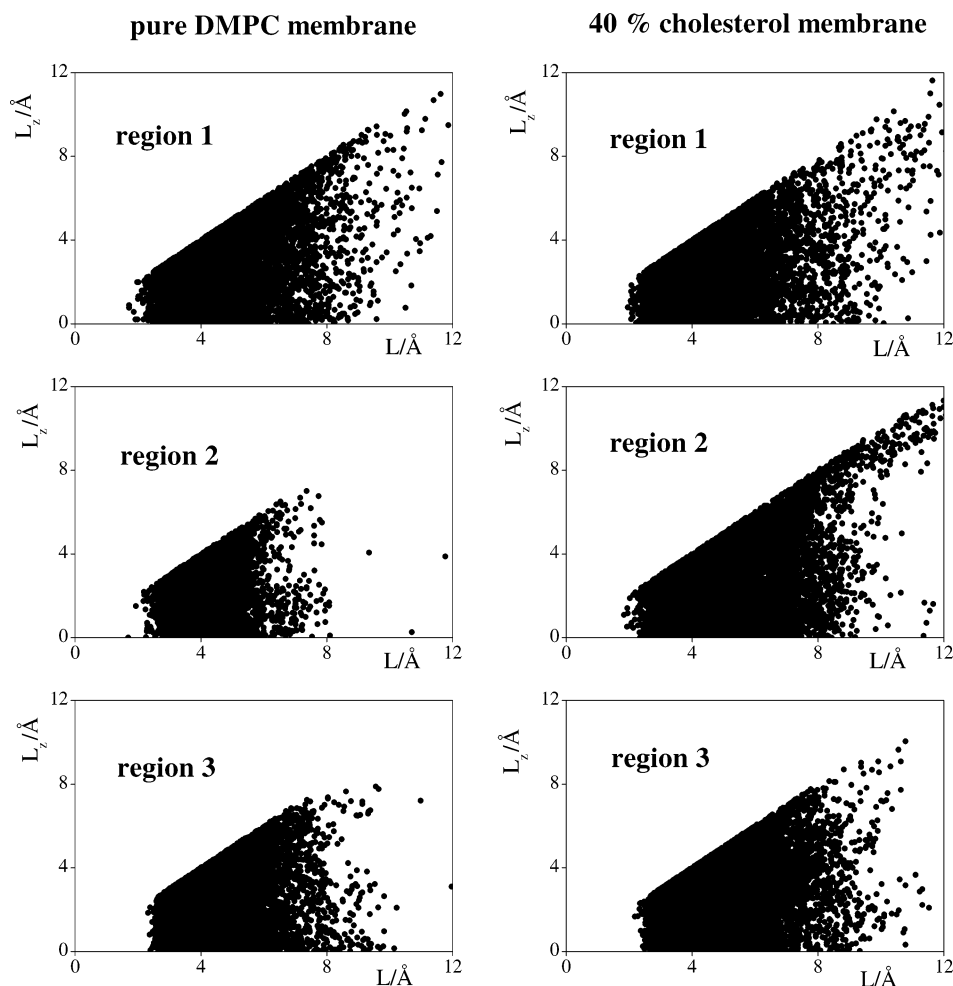


**Figure 8.** $L_z(L)$ spot diagrams of the voids accessible for probes of the radius of 1.6 Å in the three separate regions of the cholesterol-free (left) and cholesterol-rich (right) systems. In these diagrams each void is represented by a point, which corresponds to the total length of the spherocylinder representing the void $L$ and to its extension along the membrane normal axis $L_z$.

the $L_z = L$ line). Furthermore, although the large voids are lacking of such orientational preference in region 2 of the pure DMPC membrane (as seen from the fact that the points of large $L$ are scattering quite uniformly between the $L_z$ values of 0 and $L$), the presence of 40% cholesterol introduces a very strong preference of the largest voids for the orientation perpendicular to the bilayer even in this region. The preferential orientation of the voids is further analyzed in the following subsection.

The obtained values of the critical probe radius for which the voids form a percolating system are considerably smaller than the typical van der Waals radius of the atoms, indicating that there are no readily formed empty channels available in these membranes for the transport of even such small molecules as water, NO, $CO_2$, or $O_2$. However, the diffusion of these penetrants through the membrane obviously does not need empty channels across the entire membrane; parts of such channels could be opened from time to time and closed according to the dynamics of the system, facilitated also by the interaction of the penetrant with the molecules of the membrane. In light of these, the obtained $R_C^Z$ values seem to be large enough to facilitate the diffusion of small molecules through the membrane. Furthermore, the lack of broad enough empty channels spanning the entire membrane or one of its regions does not necessarily indicate the lack of similar but shorter channels, which can still largely facilitate the cross-membrane transport of small molecules. To demonstrate this, we have calculated the distribution of the extension of the voids along the membrane normal axis $L_z$ in the separate regions of the membranes studied with the

critical probe radius values of 1.3 and 1.6 Å. The obtained $P(L_z)$ distributions, shown in Figure 9 on a logarithmic scale, clearly demonstrate that the extension of these voids along the $z$ axis in region 1 can be as large as 12−13 Å, i.e., comparable with the total width of the region. Furthermore, as is seen from Figure 9, the presence of cholesterol clearly increases the $z$ extension of the broadest voids in the dense region 2. Thus, in the cholesterol-rich system voids detected with the $R_{probe}$ values of 1.3 and 1.6 Å that are extending 12.5 and 14.5 Å, respectively, along the $z$ axis can still be observed. This finding is in accordance with our previous observation about the existence of rather large voids of elongated shapes and suggests that rather broad and long empty channels extending along the bilayer normal axis are present in the membranes. It also helps explain the lowering of the barriers in the cross-membrane free-energy profiles of $CHCl_3$ and $CO_2$ by cholesterol observed in our previous work.[24] The effect of such channels can be of particular importance in the permeation of polar penetrants (e.g., water, $NH_3$, and formamide, etc.), since their solvation free energies are 30−60 kJ/mol higher in the apolar part of the membrane than in the aqueous phase.[24,31] Thus, according to the solubility−diffusion model of Marrink and Berendsen,[29,30] the membrane can only be sufficiently permeable for these penetrants if they can diffuse fast enough through the apolar phase, where their solvation free energy is high. The relatively long wide empty channels present in this region along the membrane normal axis can largely facilitate the fast permeation of the penetrants
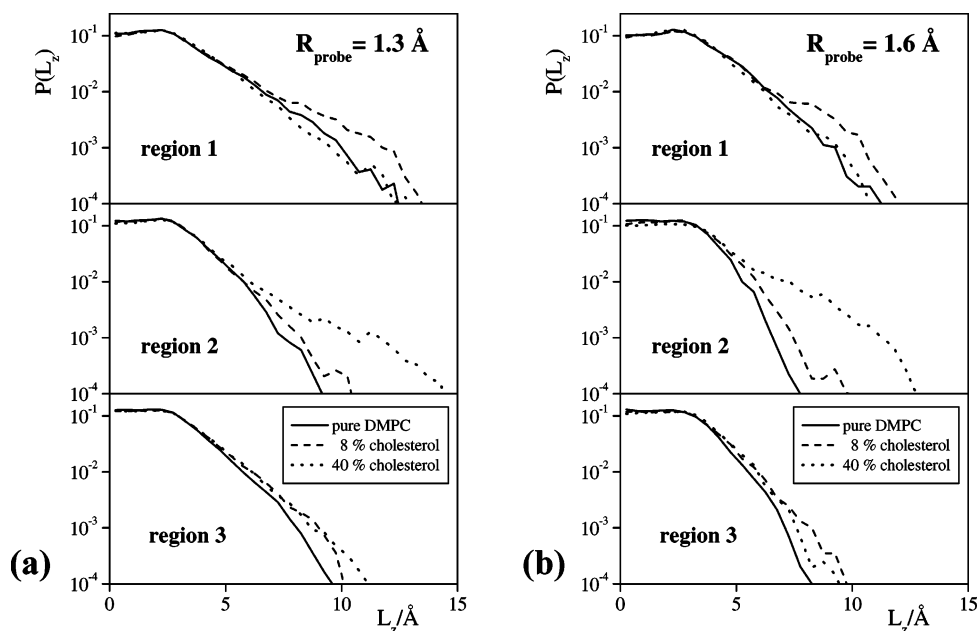
**Figure 9.** Distribution of the extension of the spherocylinders representing the voids accessible for a probe of the radius of (a) 1.3 and (b) 1.6 Å along the membrane normal axis in the three separate regions of the membranes simulated, shown on a logarithmic scale: solid lines, cholesterol-free system; dashed lines. cholesterol-poor system; dotted lines, cholesterol-rich system.
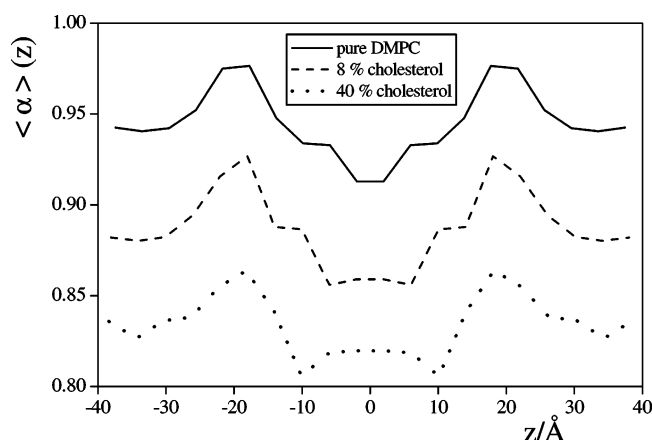


**Figure 10.** Profile of the sphericity parameter $\alpha$ of the voids across the three membranes investigated: solid lines, cholesterol-free system; dashed lines, cholesterol-poor system; dotted lines, cholesterol-rich system. All of the profiles shown are symmetrized over the two sides of the bilayers. The results of the cholesterol-poor and cholesterol-free systems are shifted by 0.05 and 0.1 units, respectively.

**Figure 11.** Profile of the orientational parameter $\cos \gamma$ of the voids across the three membranes investigated: solid lines, cholesterol-free system; dashed lines, cholesterol-poor system; dotted lines, cholesterol-rich system. All of the profiles shown are symmetrized over the two sides of the bilayers. The results of the cholesterol-poor and cholesterol-free systems are shifted by 0.05 and 0.1 units, respectively.

through this region and hence can be of key importance in the cross-membrane transport of small, polar molecules.

**3.4. Shape and Orientation of the Voids.** To analyze the shape and orientation of the voids present in the systems studied, we have represented them by spherocylinders,[36,37] as described briefly in a previous subsection. The shape of the voids is characterized by their sphericity parameter $\alpha$ (see eq 2), whereas the orientation of a void relative to the bilayer is described by the cosine of the angle $\gamma$ formed by the axis of the spherocylinder representing the void and the membrane normal axis $z$. To describe the variation of the sphericity and preferential orientation of the voids along the membrane normal axis, we have calculated the profile of $\langle\alpha\rangle$ and $\langle\cos \gamma\rangle$ across the three membranes investigated.

The $\langle\alpha\rangle(z)$ and $\langle\cos \gamma\rangle(z)$ profiles, symmetrized over the two sides of the bilayers, are shown in Figures 10 and 11, respectively, as obtained with the $R_{probe}$ value of 1.3 Å. Different $R_{probe}$ values resulted in rather similar curves. The obtained $\langle\alpha\rangle(z)$ functions correlate, in general, very well with the mass
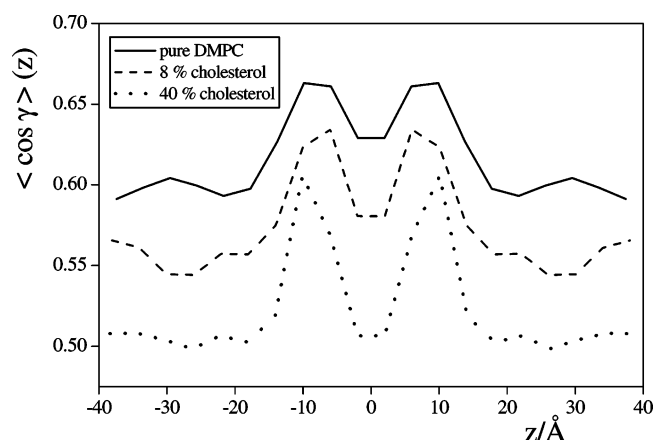
density profiles of the systems (see Figure 2) and with the partial profiles of the free volume corresponding to large enough $R_{probe}$ values (see the lower panels of Figure 1). Thus, at regions of higher densities the voids are, on average, more spherical, irrespective of the composition of the region. This finding can be explained by our above conclusion that large voids are of elongated shapes: regions of lower densities contain larger and therefore also longer (i.e., less spherical) voids, resulting in a smaller average value of the sphericity parameter $\alpha$.

When comparing the $\langle\alpha\rangle(z)$ profiles corresponding to membranes of different cholesterol content, a systematic change is observed in the central part of the bilayer. Namely, the shoulders of the $\langle\alpha\rangle(z)$ function at about ±10 Å and the clear minimum of $\langle\alpha\rangle(z)$ in the middle of the pure DMPC system develop to clear minima and a small maximum, respectively, in the cholesterol-rich system, indicating that the voids that are in the middle of the bilayer become more spherical, whereas those located about 10 Å away from the bilayer center, i.e., in the $z$
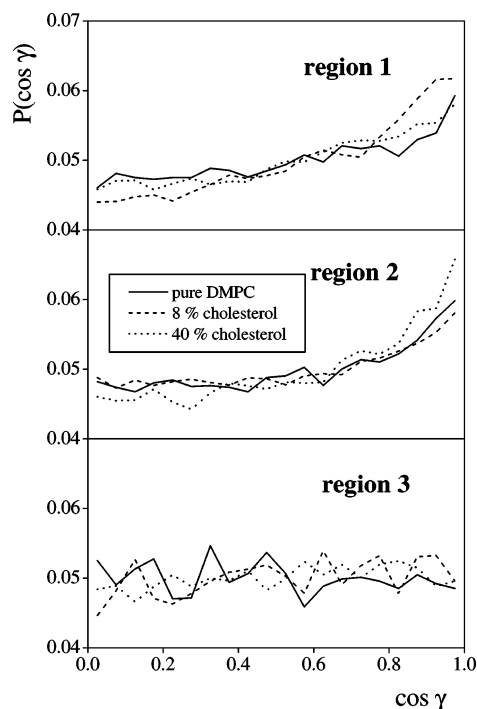
**Figure 12.** Cosine distribution of the angle $\gamma$ formed by the axis of the spherocylinders representing the voids that are accessible for a spherical probe of the radius of 1.3 Å and the membrane normal axis $z$, as obtained in the three separate regions of the three systems investigated.

range of the cholesterol rings (see Figure 2), become less spherical with increasing cholesterol content.

The obtained $\langle \cos \gamma \rangle(z)$ profiles also correlate well with the above picture. In interpreting these curves it should be noted that the two ends of a spherocylinder are equivalent, and hence the angle $\gamma$ can always be chosen not to exceed 90°, and thus $\langle \cos \gamma \rangle \geq 0$ holds. Therefore, uncorrelated orientation of the voids with the axis $z$ results in the $\langle \cos \gamma \rangle$ value of 0.5. However, since the mean value of $\cos \gamma$ does not describe its distribution, the $\langle \cos \gamma \rangle = 0.5$ value can, in principle, also correspond to the preference of the $\gamma$ value of 60° as well as to various complex orientational preferences in which the contribution of the orientations close to the parallel and to the perpendicular alignments with the membrane normal axis are equal. Similarly, the $\langle \cos \gamma \rangle$ values that are larger or smaller than 0.5 do not necessarily indicate the preference of the parallel or perpendicular alignment, respectively, with the $z$ axis; they only reflect that the orientation of the voids is closer, on average, to one of these extreme alignments than to the other one. To exclude the possibility of any kind of complex, multiple orientational preferences of the voids as well as of the preference of any type of tilted orientations, we have also calculated the distribution of $\cos \gamma$ in the three separate regions of the membranes investigated. The distributions obtained, shown in Figure 12, are indeed either monotonic, having the maximum at $\cos \gamma = 1$, or uniform (i.e., fluctuating around a constant value). This means that in our case $\langle \cos \gamma \rangle \approx 0.5$ indeed indicates uncorrelated orientation of the voids with the membrane, whereas $\langle \cos \gamma \rangle > 0.5$ reflects clearly the preference of the alignment parallel with the membrane normal axis $z$. This fact makes the interpretation of the obtained $\langle \cos \gamma \rangle(z)$ profiles considerably simpler.

Not surprisingly, in the aqueous phase of the membranes the voids are oriented in an isotropic way, as the $\langle \cos \gamma \rangle(z)$ profiles always fluctuate around 0.5 here (see Figure 11). The profiles

show a maximum around the $z$ values of $\pm 10$ Å, i.e., in that part of the membrane where the outer segments of the DMPC tails as well as the cholesterol rings are located, showing that here the preferential orientation of the voids is parallel with the membrane normal axis $z$. In the central part of the membranes the $\langle \cos \gamma \rangle(z)$ curves go through a minimum, still being larger than 0.5 in the cholesterol-free and cholesterol-poor systems, indicating that the voids are still oriented preferentially parallel with the membrane normal axis, although this preference is certainly weaker than in the $z$ range around $\pm 10$ Å. On the other hand, the value of $\langle \cos \gamma \rangle$ drops to about 0.5 in the middle of the cholesterol-rich membrane, showing that here the orientation of the voids is already isotropic. It is also seen that the presence of cholesterol influences the orientation of the voids in these two parts of the membrane in an opposite way: with increasing cholesterol concentration the preference for the parallel alignment with the $z$ axis becomes considerably stronger among the voids located in the region of the cholesterol rings, at about 10 Å away from the bilayer center, whereas it becomes clearly weaker in the middle part of the membrane, and even disappears completely in the system containing 40% cholesterol.

Finally, it should be noted that the orientation of the voids is strongly correlated with the orientation of the lipid tails and cholesterol molecules. As it has been found in our previous study,[23] preference for the parallel alignment with the membrane normal axis $z$ is (i) clearly stronger for the cholesterol rings than for the DMPC tails, (ii) becomes weaker along the DMPC tails as getting farther from the glycerol backbone of the molecule, and (iii) becomes weaker for the segments of the DMPC tails that are located close to the center of the bilayer with increasing cholesterol concentration (see Figures 9 and 11 of ref 23). These results suggest that the preference of the voids located in the hydrocarbon phase of the membranes for the parallel alignment with the membrane normal axis is imposed by the similar orientational preference of the molecules among which these voids are located in this part of the membrane.

## 4. Summary and Conclusions

In this study the capability of the Voronoi−Delaunay method is demonstrated by analyzing the properties of the interatomic voids in DMPC/cholesterol mixed membranes of various compositions in detail. The results obtained clearly show that there is a strong correlation between the spatial distribution of the voids and that of the atoms[23] in the systems. Thus, the distribution of the voids accessible for large enough spherical probes along the membrane normal axis correlates well with the density profile of the systems: in regions of lower densities the fraction of the accessible free volume is clearly higher than in the regions of higher densities. The situation is, however, not that clear when all the empty space (i.e., the entire space that is not covered by the atomic spheres) is taken into account. Thus, the highest fraction of the empty space is clearly found in the aqueous part of the membranes, although the density is higher here than in the apolar region,[23] indicating that the empty space is distributed in a more uniform way among the water molecules than among the hydrocarbon chains. This situation is, however, reverted by increasing the radius of the spherical probe used to detect the voids. Thus, the fraction of the free volume accessible for the probe becomes equal in the aqueous and apolar phases of the cholesterol-free and cholesterol-rich membranes for the probe radii of 1.3 and 1.6 Å, respectively.

Clear correlation is observed also between the orientation of the voids and that of the molecules among which they are located: the voids located in the hydrocarbon phase of the

Interatomic Voids in DMPC/Cholesterol Membranes

*J. Phys. Chem. B, Vol. 109, No. 34, 2005* **16501**

membranes, similarly to the apolar tails of the molecules,[23] prefer to align perpendicularly to the plane of the membrane. Similarly to the orientational preference of the molecules, this preference becomes also stronger with increasing cholesterol concentrations and is weaker in the middle of the membranes than in the region where the cholesterol rings are located.

The present analysis has revealed the existence of rather large voids in the membranes. Considering the fact that the volume of these voids can be an order of magnitude larger than those of the largest spherical cavities present, we can conclude that large voids are always elongated channels rather than big holes. This finding is clearly confirmed by the observed strong correlation between the volume and length of the voids. The presence of these large elongated voids as well as of the considerably narrower empty channels spanning the entire membrane can be of great importance in the cross-membrane permeation process of small, neutral penetrants, many of which are of physiological relevance (e.g., water, $CO_2$, $O_2$, NO, and $NH_3$, etc.). Although the existing empty channels that are spanning the entire membrane are obviously not broad enough to let even the smallest penetrants go readily through them, broad enough channels that are spanning $10-15$ Å wide slices of the membrane along its normal axis can be found both in the dense region of the headgroups and in the apolar membrane region. The effect of these channels can be of particular importance in the permeation process of polar penetrants, for which the solvation free energy barrier, located in the middle of the membrane, is about $30-60$ kJ/mol high,[24] and hence, according to the solubility−diffusion model of Marrink and Berendsen,[29,30] the membrane can only be sufficiently permeable for them if they can diffuse fast enough through this region.

The presence of cholesterol is found to affect the properties of the voids differently in different parts of the membrane. First, the empty space is organized in a more compact way, forming larger voids that are accessible for larger probes in the presence than in the absence of cholesterol. This effect is most pronounced in the dense region of the headgroups, where the fraction of the empty space becomes noticeably higher in the presence of even a small amount of cholesterol and where the voids of the size of $150-400$ Å$^3$, accessible for reasonably large probes, appear only in the presence of a large amount of cholesterol. In the $z$ range of the rigid cholesterol rings the fraction of the voids accessible for large probes becomes higher, the voids themselves become more elongated, and their preference for the parallel alignment with the membrane normal axis becomes stronger with increasing cholesterol concentration. On the other hand, the increasing cholesterol content of the membrane makes the voids, on average, more spherical and their orientation more isotropic in the middle of the bilayer, among the chain terminal $CH_3$ groups.

## References and Notes

(1) El-Sayed, M. Y.; Guiton, T. A.; Fayer, M. D. *Biochemistry* **1986**, *25*, 4825.

(2) Subczynski, W. K.; Wisniewska, A.; Yin, J.-J.; Hyde, J. S.; Kusumi, A. *Biochemistry* **1994**, *33*, 7670.

(3) Sackmann, E. In *Structure and Dynamics of Membranes*; Lipowsky R., Sackmann, E., Eds.; Elsevier: Amsterdam, 1995; pp 1−64.

(4) McMullen, T. P. W.; McElhaney, R. N. *Biochim. Biophys. Acta* **1995**, *1234*, 90.

(5) McMullen, T. P. W.; McElhaney, R. N. *Curr. Opin. Colloid Interface Sci.* **1996**, *1*, 83.

(6) Xiang, T.-X.; Anderson, B. D. *Biophys. J.* **1997**, *72*, 223.

(7) Méléard, P.; Gerbeaud, C.; Pott, T.; Fernandez-Puente, L.; Bivas, I.; Mitov, M. D.; Dufourcq, J.; Bothorel, P. *Biophys. J.* **1997**, *72*, 2616.

(8) Smaby, J. M.; Momsen, M. M.; Brockman, H. L.; Brown, R. E. *Biophys. J.* **1997**, *73*, 1492.

(9) Radhakrishnan, A.; McConnell, H. M. *J. Am. Chem. Soc.* **1999**, *121*, 486.

(10) Keller, S. L.; McConnell, H. M. *Phys. Rev. Lett.* **1999**, *82*, 1602.

(11) Richter, F.; Finegold, L.; Rapp, G. *Phys. Rev. E* **1999**, *59*, 3483.

(12) Weisman, S.; Hirsch-Lerner, D.; Barenholz, Y.; Talmon, Y. *Biophys. J.* **2004**, *87*, 609.

(13) Edholm, O.; Nyberg, A. M. *Biophys. J.* **1992**, *63*, 1081.

(14) Robinson, A. J.; Richards, W. G.; Thomas, P. J.; Hann, M. M. *Biophys. J.* **1995**, *68*, 164.

(15) Gabdouline R. R.; Vanderkooi, G.; Zheng, C. *J. Phys. Chem.* **1996**, *100*, 15942.

(16) Tu, K.; Klein, M. L.; Tobias, D. J. *Biophys. J.* **1998**, *75*, 2147.

(17) Smondyrev, A. M.; Berkowitz, M. L. *Biophys. J.* **1999**, *77*, 2075.

(18) Pasenkiewicz-Gierula, M.; Róg, T.; Kitamura, K.; Kusumi, A. *Biophys. J.* **2000**, *78*, 1376.

(19) Smondyrev, A. M.; Berkowitz, M. L. *Biophys. J.* **2000**, *78*, 1672.

(20) Chiu, S. W.; Jakobsson, E.; Scott, H. L. *J. Chem. Phys.* **2001**, *114*, 5435.

(21) Chiu, S. W.; Jakobsson, E.; Mashl, R. J.; Scott, H. L. *Biophys. J.* **2002**, *83*, 1842.

(22) Hofsäss, C.; Lindahl, E.; Edholm, O. *Biophys. J.* **2003**, *84*, 2192.

(23) Jedlovszky, P.; Mezei, M. *J. Phys. Chem. B* **2003**, *107*, 5311.

(24) Jedlovszky, P.; Mezei, M. *J. Phys. Chem. B* **2003**, *107*, 5322.

(25) Jedlovszky, P.; Medvedev, N. N.; Mezei, M. *J. Phys. Chem. B* **2004**, *108*, 465.

(26) Falck, E.; Patra, M.; Karttunen, M.; Hyvönen, M. T.; Vattulainen, I. *Biophys. J.* **2004**, *87*, 1076.

(27) Pandit, S. A.; Vasudevan, S.; Chiu, S. W.; Mashl, R. J.; Jakobsson, E.; Scott, H. L. *Biophys. J.* **2004**, *87*, 1092.

(28) Falck, E.; Patra, M.; Karttunen, M.; Hyvönen, M. T.; Vattulainen, I. *J. Chem. Phys.* **2004**, *121*, 12676.

(29) Marrink S. J.; Berendsen, H. J. C. *J. Phys. Chem.* **1994**, *98*, 4155.

(30) Marrink S. J.; Berendsen, H. J. C. *J. Phys. Chem.* **1996**, *100*, 16729.

(31) Jedlovszky, P.; Mezei, M. *J. Am. Chem. Soc.* **2000**, *122*, 5125.

(32) Marrink, S. J.; Sok, R. M.; Berendsen, H. J. C. *J. Chem. Phys.* **1996**, *104*, 9090.

(33) Voronoi, G. F. *J. Reine Angew. Math.* **1908**, *134*, 198.

(34) Delaunay, B. N. *Proceedings of the Mathematics Congress*, Toronto, Aug 11−16, 1924; University of Toronto Press: Toronto, Canada, 1928; pp 695−700.

(35) Medvedev, N. N. *The Voronoi-Delaunay Method in the Structural Investigation of Non-crystalline Systems*; SB RAS: Novosibirsk, Russia, 2000 (in Russian).

(36) Anikeenko, A. V.; Alinchenko, M. G.; Voloshin, V. P.; Medvedev, N. N.; Gavrilova, M. L.; Jedlovszky, P. In *Proceedings of the 4th Workshop of Computational Geometry and Applications*; Lecture Notes in Computer Science 3045; Springer-Verlag: Berlin, 2004; Vol. III, pp 217−226.

(37) Alinchenko, M. G.; Anikeenko, A. V.; Medvedev N. N.; Voloshin, V. P.; Mezei, M.; Jedlovszky, P. *J. Phys. Chem. B* **2004**, *108*, 19056.

(38) Rabinovich, A. L.; Balabaev, N. K.; Alinchenko, M. G.; Voloshin, V. P.; Medvedev, N. N.; Jedlovszky, P. *J. Chem. Phys.* **2005**, *122*, 084906.

(39) Okabe, A.; Boots, B.; Sugihara, K.; Chiu, S. N. *Spatial Tessellations: Concepts and Applications of Voronoi Diagrams*; Wiley: Chichester, U.K., 2000.

(40) Anishchik, S. V.; Medvedev, N. N. *Phys. Rev. Lett.* **1995**, *75*, 4314.

(41) Gerstein, M.; Tsai, J.; Levitt, M. *J. Mol. Biol.* **1995**, *249*, 955.

(42) Goede, A.; Preissner, R.; Froemmel, C. *J. Comput. Chem.* **1997**, *18*, 1113.

(43) Will, H. M. Technical Reports No. 300 and No. 302, 1998, ETH Zürich−URL: ftp:// ftp.inf.ethz.ch/pub/publications/tech-reports.

(44) Richard, P.; Oger, L.; Troadec, J. P.; Gervois, A. *Eur. Phys. J. E* **2001**, *6*, 295.

(45) Rother, K.; Preissner, R.; Goede, A.; Froemmel C. *Bioinformatics* **2003**, *19*, 2112.

(46) Hilderbrand, P. W.; Rother, K.; Goeder, A.; Preissner, R.; Froemmel, C. *Biophys. J.* **2005**, *88*, 1970.

(47) Gellatly B. J.; Finney, J. L. *J. Non-Cryst. Solids* **1982**, *50*, 313.

(48) Sadoc, J. F.; Jullien, R.; Rivier, N. *Eur. Phys. J. B* **2003**, *33*, 355.

(49) Naberukhin, Y. I.; Voloshin, V. P.; Medvedev, N. N. *Mol. Phys.* **1991**, *73*, 917.

(50) Voloshin, V. P.; Naberukhin, Y. I.; Medvedev, N. N. *Zh. Phys. Khimii* **1992**, *66*, 155 (in Russian).

(51) Medvedev, N. N. In *Voronoi Impact on Modern Science*; Samoilenko, A. M., Ed.; Institute of Mathematics: Kiev, Ukraine, 1998; Vol. 2, p 164.

(52) Jorgensen, W. L.; Chandrashekar, J.; Madura, J. D.; Impey, R.; Klein, M. L. *J. Chem. Phys.* **1983**, *79*, 926.

(53) Schlenkirch, M.; Brickmann, J.; MacKerell, A. D., Jr.; Karplus, M. In *Biological Membranes*; Merz, K. M., Roux, B., Eds.; Birkhäuser: Boston, 1996; pp 31−82.

(54) Mezei, M. MMC Program at URL: http://inka.mssm.edu/~mezei/mmc. MMC is a program for the modeling of molecular assemblies in the condensed phase using Markov-chain Monte Carlo method. The simulations can sample positional, orientational, and torsional degrees of freedom in the canonical, isobaric−isothermal, and grand-canonical ensembles.

(55) Jedlovszky, P.; Mezei, M. *J. Chem. Phys.* **1999**, *111*, 10770.

(56) Mezei, M. *J. Comput. Phys.* **1983**, *39*, 128.

(57) Jedlovszky, P.; Mezei, M. *Mol. Phys.* **1999**, *96*, 293.

(58) Bernal, J. D. *Proc. R. Soc. London* **1964**, *A280*, 299.

(59) Rogers, C. A. *Packing and Covering*; Cambridge University Press: London, 1964.

(60) Hsu C. S.; Rahman, A. J. *J. Chem. Phys.* **1979**, *70*, 5234.

(61) Hsu C. S.; Rahman, A. J. *J. Chem. Phys.* **1979**, *71*, 4974.

(62) Medvedev, N. N.; Geiger, A.; Brostow, W. *J. Chem. Phys.* **1990**, *93*, 8337.

(63) Luchnikov, V. A.; Medvedev, N. N.; Appelhagen, A.; Geiger, A. *Mol. Phys.* **1996**, *88*, 1337.

(64) Brostow, W.; Chybicki, M.; Laskowski, R.; Rybicki, J. *Phys. Rev. B* **1998**, *57*, 13448.

(65) Baranyai, A.; Ruff, I. *J. Chem. Phys.* **1986**, *85*, 365.

(66) Pusztai, L.; Baranyai, A.; Ruff, I. *J. Phys. C* **1988**, *21*, 3687.

(67) Wilson M.; Madden, P. A. *Phys. Rev. Lett.* **1998**, *80*, 532.

(68) Finney, J. L. *Proc. R. Soc. London* **1970**, *319*, 479.

(69) Finney, J. L. *Proc. R. Soc. London* **1970**, *319*, 495.

(70) Hiwatari, Y.; Saito, T.; Ueda, A. *J. Chem. Phys.* **1984**, *81*, 6044.

(71) Medvedev, N. N.; Naberukhin, Y. I. *J. Non-Cryst. Solids* **1987**, *94*, 402.

(72) Bryant S.; Blunt, M. *Phys. Rev. A* **1992**, *46*, 2004.

(73) Oger L.; Gervois, A.; Troadec, J. P.; Rivier, N. *Philos. Mag. B* **1996**, *74*, 177.

(74) Medvedev, N. N.; Naberukhin, Y. I. *J. Phys. A* 1**988**, *21*, L247.

(75) Gil Montoro, J. C.; Abascal, J. L. F. *J. Phys. Chem.* **1993**, *97*, 4211.

(76) Voloshin, V. P.; Naberuknun, Y. I.; Medvedev, N. N.; Shik Jhon, M. *J. Chem. Phys.* **1995**, *102*, 4981.

(77) Ruocco, G.; Sampoli, M.; Vallauri, R. *J. Chem. Phys.* **1992**, *96*, 6167.

(78) Ruocco, G.; Sampoli, M.; Torcini, A.; Vallauri, R. *J. Chem. Phys.* **1993**, *99*, 8095.

(79) Shih, J. P.; Sheu, S. Y.; Mou, C. Y. *J. Chem. Phys.* **1994**, *100*, 2202.

(80) Yeh Y.; Mou, C. Y. *J. Phys. Chem. B* **1999**, *103*, 3699.

(81) Jedlovszky, P. *J. Chem. Phys.* **1999**, *111*, 5975.

(82) Jedlovszky, P. *J. Chem. Phys.* **2000**, *113*, 9113.

(83) Edelsbrunner, H.; Mücke, E. *A. C. M. Trans. Graphics* **1994**, *13*, 43.

(84) Liang, J.; Edelsbrunner, H.; Fu, P.; Sudhakar, P. V.; Subramaniam S. *Proteins: Struct., Funct., Genet.* **1998**, *33*, 1.

(85) Liang, J.; Edelsbrunner, H.; Fu, P.; Sudhakar, P. V.; Subramaniam S. *Proteins: Struct., Funct., Genet.* **1998**, *33*, 18.